Supporting Information

The Central Role of Tilted Anisotropy for Field-Free Spin-Orbit Torque Switching of Perpendicular Magnetization

Chen-Yu Hu[†]*, Wei-De Chen*[†]*, Yan-Ting Liu, Chao-Chun Huang, and Chi-Feng Pai*[*]

Chen-Yu Hu, Wei-De Chen, Yan-Ting Liu, Chao-Chun Huang, and Chi-Feng Pai

Department of Materials Science and Engineering, National Taiwan University

Taipei 10617, Taiwan

E-mail: cfpai@ntu.edu.tw

Chi-Feng Pai

Center of Atomic Initiative for New Materials, National Taiwan University

Center for Quantum Science and Engineering, National Taiwan University

Taipei 10617, Taiwan

1. Wedge effect in films prepared on wedge-shape holder

The thickness difference across the films prepared by oblique angle deposition was characterized using an atomic force microscope (AFM). **Fig.** S1(a) demonstrates the height profile of a step across the SiO_2 substrate and the obliquely-deposited Pt film, which was prepared on a 40°-holder with a growth time of 300 s and sputtering power of 30 W. The average thickness gradient along the *y* direction is given as $\Delta h/\Delta y = 0.06\ \mathrm{nm/\mu m}$ with average height of 13.1 nm. Therefore, in the 5 nm thick underlayer Pt used in the $\theta_{\mathrm{dep}} = 40°$-based devices, the thickness difference across the $5\ \mathrm{\mu m}$-wide Hall channel in the transverse direction approximately is $(0.06\ \mathrm{nm/\mu m}) \times (5\ \mathrm{\mu m}) \times \frac{5\ \mathrm{nm}}{13.1\ \mathrm{nm}} = 0.1\ \mathrm{nm}$. And for the case of uniformly deposited Co layer prepared on a rotating 40°-holder, its wedge effect is investigated as well. The height profile of a step prepared with a growth time of 600 s and sputtering power of 30 W is shown in **Fig.** S1(b), which gives $\Delta h/\Delta y = -0.17\ \mathrm{nm/\mu m}$ and average height of 12.3 nm. For the 0.5 nm Co layer in the $\theta_{\mathrm{dep}} = 40°$-based devices, the estimated transverse thickness difference across the 5 μm-wide Hall channel is accordingly to be $(0.17\ \mathrm{nm/\mu m}) \times (5\ \mathrm{\mu m}) \times \frac{0.5\ \mathrm{nm}}{12.3\ \mathrm{nm}} = 0.03\ \mathrm{nm}$. Both cases imply the wedge effect are not substantial as using a wedge-shape sample holder to obliquely depositing Pt layer and uniformly depositing Co layer.

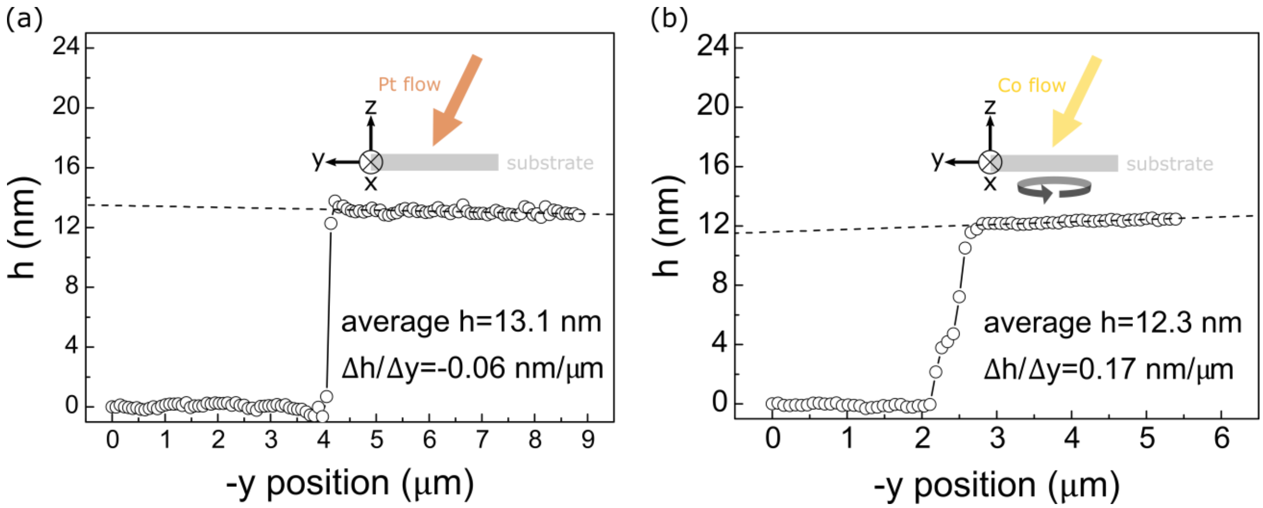

Fig. S1 Height profiles of steps crossing SiO_2 substrate and the deposited films, which were characterized by an atomic force microscope. a An obliquely deposited Pt film and **b** an uniformly deposited Co film, both are prepared on a 40°-holder. The orange and yellow arrows indicate the Pt and Co atom flow coming from the sputtering targets, respectively. The deposition angles are illustrated rather depicting the exact direction.

2. Damping-like SOT efficiency of obliquely-deposited Pt/Co/Pt layers

The damping-like SOT efficiencies (ξ_{DL}) of the uniformly and obliquely-deposited Pt/Co/Pt layers were characterized according to the framework of anomalous Hall effect (AHE) hysteresis loop shift measurement[1]. The perpendicular effective SOT field generated per applied current ($H_{\mathrm{z}}^{\mathrm{eff}}/I$) as functions of external in-plane field (H_{x}) are summarized in **Fig.** S2, where the applied current is ranging from -2.5 mA to +2.5 mA. In this small range of applied current, the estimated ξ_{DL} are given as 0.09 for $\theta_{\mathrm{dep}} = 0°$ and 0.14 for $\theta_{\mathrm{dep}} = 40°$, which are consistent with the previously reported value[2] of efficiency of Pt.

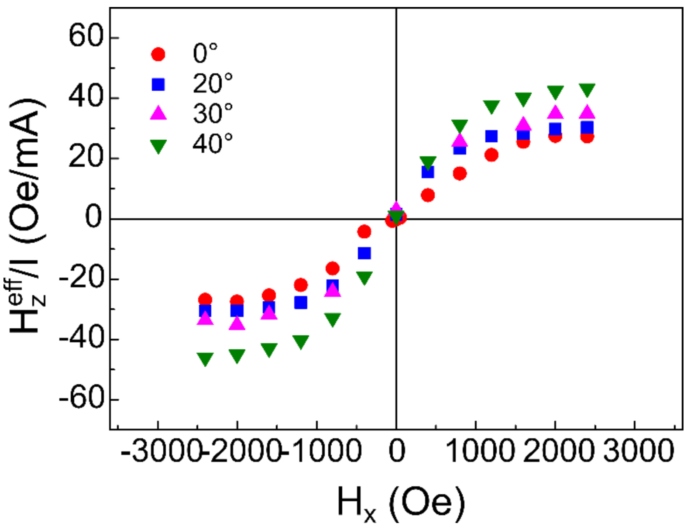

Fig. S2 DL-SOT characterization. Perpendicular SOT effective field per current (H_z^{eff}/I) varying with different longitudinal magnetic field (H_x). The data are characterized from the Pt/Co/Pt layers prepared by different deposition angle (0° to 40°).

3. Out-of-plane anisotropy field of obliquely-deposited Pt/Co/Pt layers

The value of out-of-plane anisotropy field (H_k) of the Pt/Co/Pt layers was determined through the response of out-of-plane magnetization (m_z) to the external in-plane magnetic field[3]. **Fig.** S3 shows the m_z reduction behavior of devices with and without tilted anisotropy, which are respectively prepared by $\theta_{\text{dep}} = 0°$ and 40°. In **Fig.** S3(a), the device without tilted anisotropy shows a symmetric m_z reduction behavior as applying transverse external magnetic field (H_y), which is quite different from the response of the device with tilted anisotropy shown in **Fig.** S3(b), that an out-of-plane magnetization switching happens as applying a sufficiently large H_y. Such switching is consistent with the scenario of laterally tilted anisotropy that the H_y projected onto the easy axis is non-zero for the case with tilted anisotropy. Additionally, the value of H_k can be extracted through $1/H_k = \sqrt{\left|\partial^2 m_z/\partial H_y^2\right|}$, giving H_k approximately 5824 Oe and 7432 Oe for the devices with and without tilted anisotropy, respectively. This result implies that the presence of tilted anisotropy would slightly reduce the out-of-plane anisotropy.

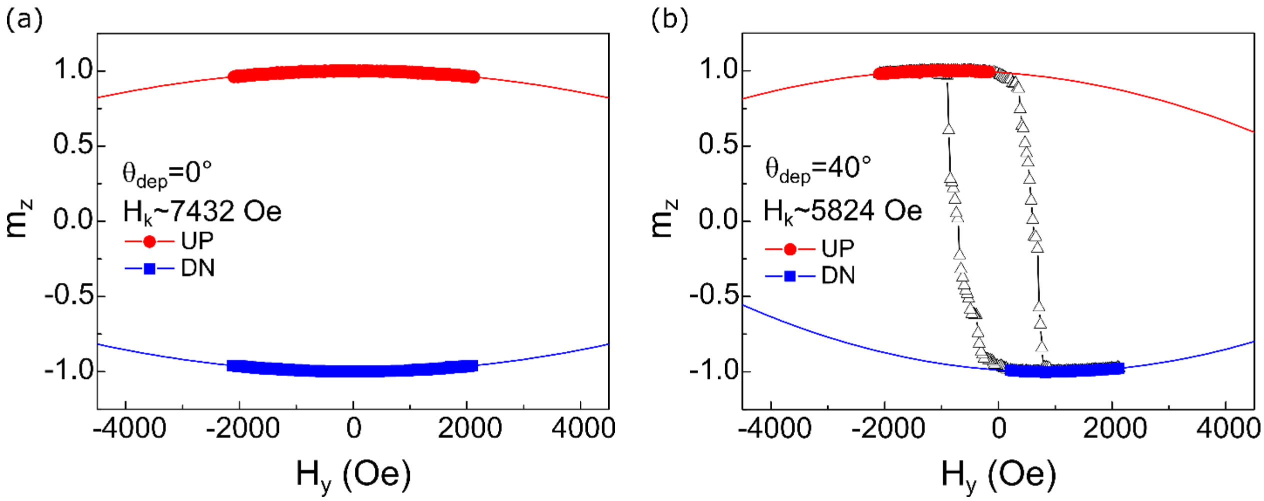

Fig. S3 Anisotropy field characterization. Response of out-of-plane magnetization (m_z) to external transverse magnetic field (H_y) of obliquely-deposited Pt/Co/Pt layers. a, b Devices without/with tilted anisotropy, which were prepared under deposition angle of 0° and 40°.

4. Pulse-width dependent field-free switching of Pt/Co/Pt layers

The pulse-width-dependent field-free switching of a $\theta_\mathrm{dep} = 40°$ device was investigated to elucidate the influence from Joule heating, where the write current pulses were generated using an arbitrary pulse generator, Model Agilent 81110A. **Fig.** S4(a) represents the reduction of critical switching current (I_c) as increasing the pulse width of write current (t_pulse) from 0.03 ms (30 μs) to 900 ms. The I_c as functions of $\ln(t_{\mathrm{pulse}}/\tau_0)$ shown in **Fig.** S4(b) demonstrates a typical linear behavior of thermal activation model[4], which is described by **Equation** S1.

$$I_c = I_{c0}\left[1 - \frac{1}{\Delta}\ln\left(\frac{t_{\mathrm{pulse}}}{\tau_0}\right)\right], \tag{S1}$$

where I_{c0} is the zero-thermal critical switching current; $\Delta = U/k_B T$ parameterizes the thermal stability to describe the energy barrier (U) between magnetically UP and DOWN state, which is normalized by the product of Boltzmann constant (k_B) and temperature (T); $\tau_0 = 1$ ns is the intrinsic attempt time.

The extracted I_{c0} and Δ respectively are given as 13.07 mA and 27.72. Additionally, the observed linear relationship implies the field-free switching in this pulse range ($t_{\mathrm{pulse}} > 0.03$ ms) is still governed by thermally-activated mechanism rather than dynamical (ballistic) switching.

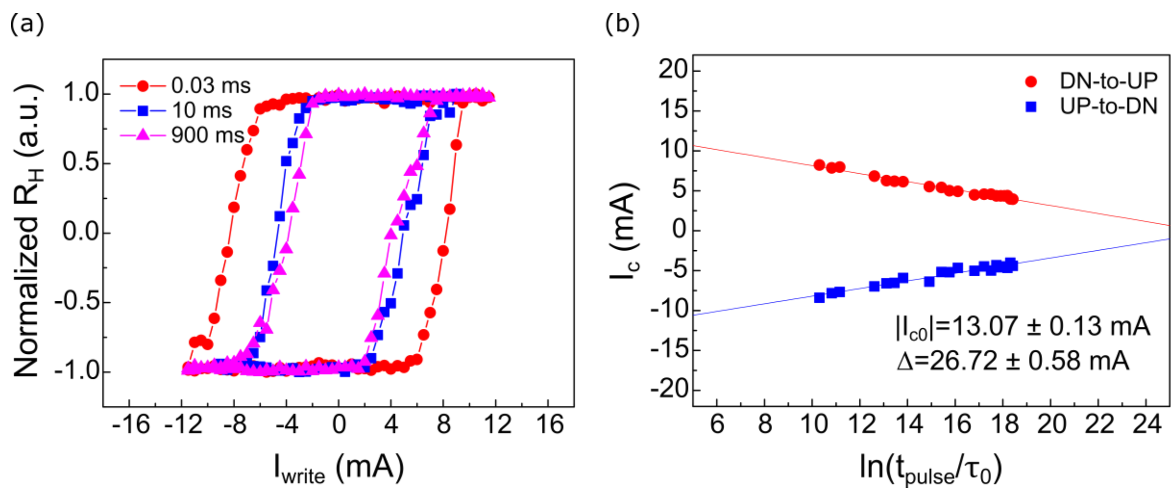

Fig. S4 Pulse-width dependent field-free switching of a device prepared by oblique angle deposition ($\boldsymbol{\theta_{\mathrm{dep}} = 40°}$). a Representative switching loops by pulse width of 0.03 ms, 10 ms and 900 ms. **b** Linear relationship between $\ln(t_{\mathrm{pulse}}/\tau_0)$ and critical switching current (I_{c}).

5. Pt/Co/Pt layers prepared by two-step fabrication

To identify which deposited layer plays a more decisive role to the resulting symmetry breaking and field-free switching, we prepared two different stacks by a two-step fabrication method, as illustrated in **Fig.** S5. For stack A (**Fig.** S5(c)), after preparing Ta(0.5)/Pt(5) layers in the same way as the devices of $\theta_{\mathrm{dep}} = 40°$ in the main text (using 40° holder and oblique angle deposition), we transferred the sample to the 0°-holder and deposited the rest of the layers, Co(0.6)/Pt(1)/Ta(2), by uniform deposition; for stack B (**Fig.** S5(d)), the Ta(0.5)/Pt(5) layers were uniformly deposited by using the 0°-holder, then transferred to the 40°-holder for the Co(0.6)/Pt(1)/Ta(2) depositions as the way of preparing the devices of $\theta_{\mathrm{dep}} = 40°$ in the main text (uniform deposition). The slightly thicker Co thickness used in these two stacks is because of the inevitable exposure to the atmosphere for Pt/Co interface when changing the holder, which changes the PMA condition in our experiments.

Compared to the devices in the main text shown in **Fig.** S5(a,b), the field-free switching results shown in **Fig.** S5(c,d) show that only stack A can still achieve current-induced field-free switching, suggesting that the obliquely deposited Pt(5) serving as underlayer governs the symmetry breaking of this system. This also rules out the possible influence or introducing extra symmetry-breaking mechanism by preparing the Co layer on a rotating wedge-shape holder.

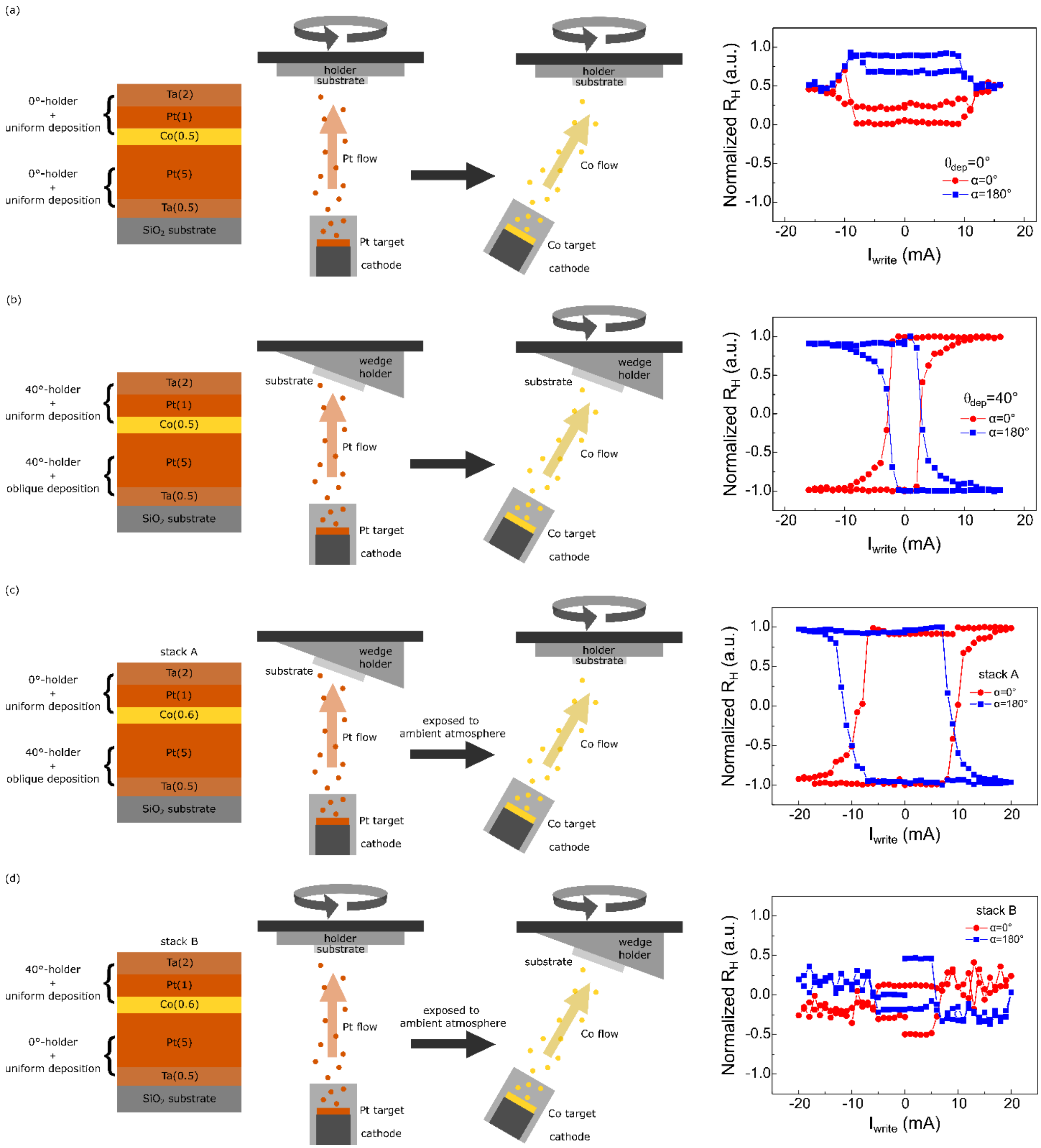

Fig. S5 The schematics of the fabrication details to prepare Pt/Co/Pt structures and the corresponding field-free switching results with α = 0°, 180° Hall bar arragement. The uniform deposition indicates the sample is rotating during the deposition; otherwise, the oblique deposition is not. **a** the 0°-devices in the main text of Ta(0.5)/Pt(5)/Co(0.5)/Pt(1)/Ta(2) fully prepared by uniform deposition on the 0°-holder. **b** the 40°-devices in the main text of obliquely deposited Ta(0.5)/Pt(5) and uniformly deposited Co(0.5)/Pt(1)/Ta(2) on the 40°-holder. **c** the stack A comprised of obliquely deposited Ta(0.5)/Pt(5) on the 40°-holder and uniformly deposited Co(0.6)/Pt(1)/Ta(2) on the 0°-holder. **d** the stack B of Ta(0.5)/Pt(5)/Co(0.6)/Pt(1)/Ta(2) fully prepared by uniform deposition on the 0°-holder.

6. Field-free switching uniformity of obliquely deposited Pt/Co/Pt layers

The device performance uniformity is verified through conducting the field-free switching measurements of two $\theta_{\mathrm{dep}} = 40°$ devices, which were positioned approximately 5 mm apart. The results depicted in **Fig.** S6 suggest that both devices are capable of field-free switching and exhibit similar values for the switching current. Consequently, concerns regarding uniformity should be of minor significance that at this scale.

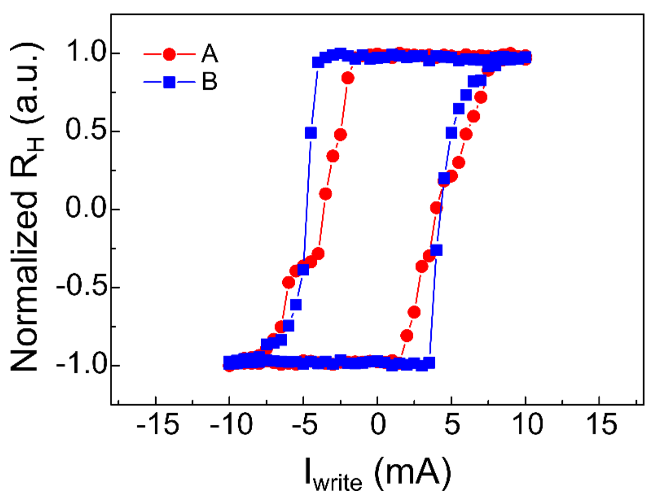

Fig S6. Switching uniformity check. Current-induced field-free switching loops of two devices prepared by $\theta_{\mathrm{dep}} = 40°$, which were positioned approximately 5 mm apart during the deposition process.

7. Switching field of spin-transfer-torque-like feature in the obliquely-deposited device

Under the zero in-plane magnetic field (H_{IP}) condition, the switching field (H_{sw}) under different applied currents (I_{applied}) in the AHE hysteresis loop measurement is defined as when the normalized Hall resistance changes its sign, and the loop center is defined as $\Delta H_{\mathrm{sw}} \equiv \frac{1}{2}(H_{\mathrm{sw}}^{\mathrm{DN-to-UP}} + H_{\mathrm{sw}}^{\mathrm{UP-to-DN}})$. **Fig.** S7 summarizes the switching behavior and shows a clear difference: a typical H_{sw} reduction from only the Joule heating for $\theta_{\mathrm{dep}} = 0°$ and a damping-like spin torque switching feature for $\theta_{\mathrm{dep}} = 40°$. Note that there is no obvious shift when the applied current I_{applied} is less than ~ 2 mA.

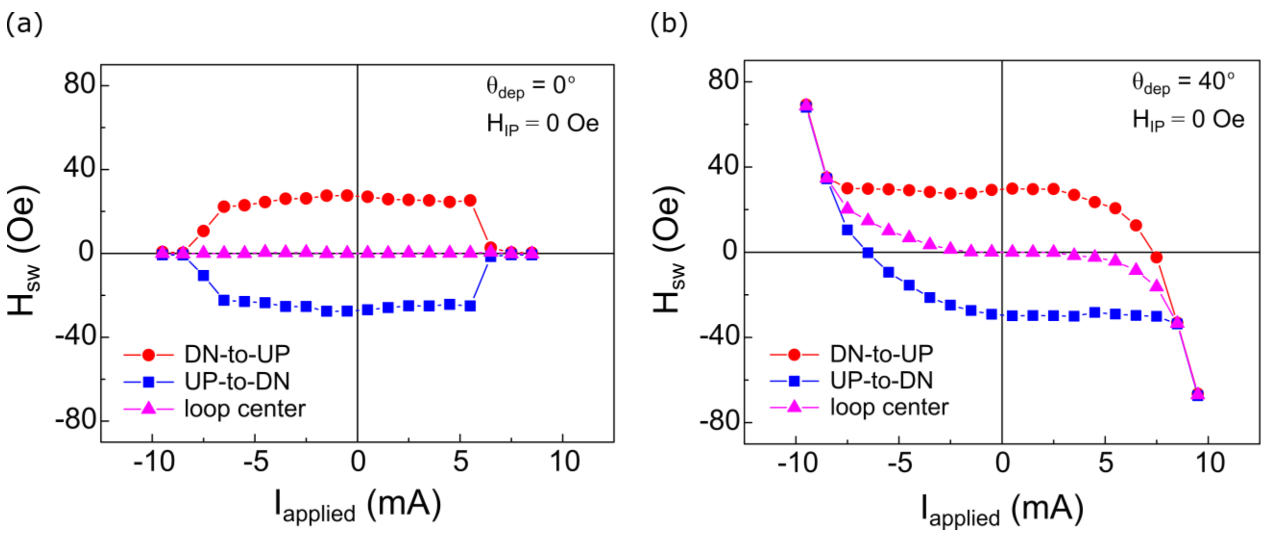

Fig. S7 The comparison of the switching field (H_{sw}) and loop center (ΔH_{sw}) under different applied current. a, b H_{sw} and ΔH_{sw} as functions of I_{applied} for the devices prepared by $\theta_{\mathrm{dep}} = 0°$ and $40°$. The measurements are characterized in an in-plane field-free condition ($H_{\mathrm{IP}} = 0$ Oe).

Reference

S1. C. F. Pai, M. Mann, A. J. Tan and G. S. D. Beach. Determination of spin torque efficiencies in heterostructures with perpendicular magnetic anisotropy. *Phys. Rev. B* **93**, 144409 (2016).

S2. C. Y. Hu and C. F. Pai. Benchmarking of Spin–Orbit Torque Switching Efficiency in Pt Alloys. *Advanced Quantum Technologies*, 2000024 (2020).

S3. S. J. Yun, E. S. Park, K. J. Lee and S. H. Lim. Accurate analysis of harmonic Hall voltage measurement for spin-orbit torques. *Npg Asia Materials* **9**, e449 (2017).

S4. R. H. Koch, J. A. Katine and J. Z. Sun. Time-resolved reversal of spin-transfer switching in a nanomagnet. *Phys. Rev. Lett.* **92**, 088302 (2004).